Smartly Aligning Nanowires by a Stretching Strategy and Their Application As Encoded Sensors

Yuchen Wu,[†] Bin Su,[†,*] and Lei Jiang[†,‡]

[†]Key Laboratory of Organic Solids, Beijing National Laboratory for Molecular Sciences, Institute of Chemistry, Chinese Academy of Sciences, Beijing, 100190, People's Republic of China and [‡]School of Chemistry and Environment, Beihang University, Beijing, 100191, People's Republic of China

ABSTRACT The nanotechnology world is being more and more attracted toward high aspect ratio one-dimensional nanostructures due to their potentials as building blocks for electronic/optical devices. Here, we propose a novel method to generate nanowire patterns with assistance of superhydrophobic flexible polydimethylsiloxane (PDMS) substrates. Micropillar gaps are tunable *via* a stretching process of the PDMS surface; thus, diverse nanowire patterns can be formed by stretching the same PDMS surface in various ways. Importantly, square nanowire loops with alternative compositions can be generated through a double-stretching process, showing an advanced methodology in controlling the alignment of nanowires. Since alternative fluorescent molecules will be quenched by diverse chemical substances, this alternative nanowire loop shows a selective detection for diverse target compounds, which greatly improves the application of this nanowire patterning approach. Furthermore, such alternative nanowire patterns can be transferred from pillar-structured surfaces to flat films, indicating further potentials in microcircuits, sensitive sensors, and other organic functional nanodevices.

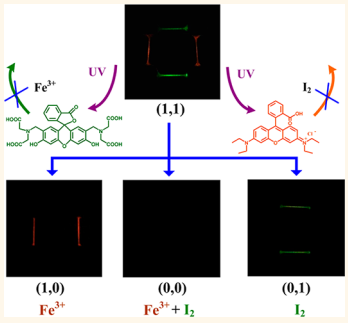

KEYWORDS: smart · fluorescence quenching · nanowire alignment · superhydrophobic · PDMS

One-dimensional (1D) organic nanostructures, which represent attractive building blocks for hierarchical assembly of electronic/optical devices, have been widely investigated.[1−9] To integrate them into functional applications, precisely aligning and positioning 1D nanostructures on the desired substrates is a prerequisite.[10,11] Many efforts have been made in the past decades, such as electric/magnetic force introduction,[12,13] geometry-restricted evaporation induction,[14−16] nanoimprint lithography,[17−19] Langmuir−Blodgett approach,[20−22] flow-assisted alignment,[23,24] and bubble-blown technique.[25] Although these efforts have dramatic abilities to force 1D nanostructures toward one direction in a large scale, the position of each nanostructure is random in the aligning matrix, which greatly prevents further effective butt-joint formation with metallic electrodes and integration into functional devices. Recently, our group has developed a facile method to precisely align and position 1D organic nanostructures, both polymer[26] and small molecules,[27] with the assistance of highly adhesive superhydrophobic pillar-structured silicon substrates. However, the positioning of nanowires is dominated by predesigned silicon micropillar arrangements, indicating invariant nanowire alignment while the substrate is fixed. Since there is certainly a practical need for nanowire patterns with tunable alignments, employing a series of substrates with diverse pillar arrangements is undoubtedly the only choice, which represents an uneconomical and complex process. Therefore, developing a simple yet efficient strategy for smart alignment of nanowires on one substrate presents an important and timely issue.

Flexible polydimethylsiloxane (PDMS) surfaces exhibit unique tensility that has been employed in various fields, such as on-demand colloidal sphere patterning,[28] stretchable battery electrodes,[29,30] and energy harvesting.[31] Following the external stretching behavior of a PDMS film, the gaps of micro/nanostructures on the film might increase accordingly. Since the micropillar gap plays a key role in dominating the nanowire formation,[26] it is possible to elaborately control the alignment of nanowires *via* such a stretching process. Thus, we replaced rigid pillar-structured silicon substrates by flexible PDMS surfaces with the same geometrical structures through a double hot embossing technique.[32] Due to the tunable gap values through applying different tensile strength, this strategy might overcome the drawbacks of rigid substrates and open a new route in smartly controlling nanowire alignment.

* Address correspondence to subin0000@iccas.ac.cn.

Received for review July 11, 2012 and accepted September 17, 2012.

Published online September 17, 2012
10.1021/nn303098n

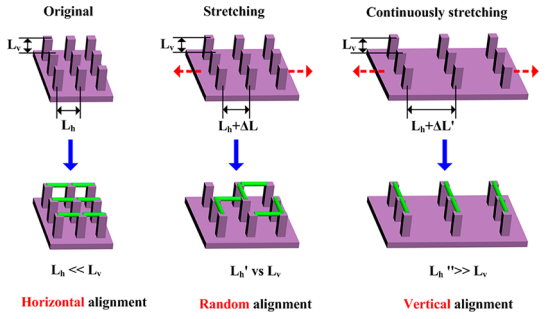

Scheme 1. Smart alignment of nanowires can be performed by stretching a flexible polydimethylsiloxane (PDMS) pillar-structured surface. Following unidirectional shrinkage behaviour of this flexible polymeric film, the horizontal pillar gap (L_h) might increase dramatically, while the vertical gap (L_v) remains. After placing similar droplets of diluted polyvinyl-formal (PVF) solution on the surfaces with diverse tensile strengths, the alignment of the nanowires can be tailored from a horizontal orientation (left) to a random patterning (middle) and then to a vertical direction (right).

Herein, we report a simple yet effective approach for smart alignment of nanowires by stretching a flexible PDMS pillar-structured surface. Micropillar gaps are tunable *via* a stretching process of the PDMS surface; thus, the alignment of nanowires can be changed according to the tailored pillar arrangements. Since nanowires are inclined to a position between the closer micropillars, diverse nanowire patterns might form by stretching the same PDMS surface in various ways. Importantly, a square nanowire loop consisting of alternative calcein/rhodamine B can be generated through a double-stretching processes. Because these two fluorescent molecules might be quenched with diverse target compounds, an encoded sensor can thus be generated based on selective quenching reactions. Furthermore, such alternative nanowire patterns can be transferred from pillar-structured surfaces to flat films, indicating wide applications in organic functional devices, especially encoded chemical sensors.[33−35]

RESULTS AND DISCUSSION

A PDMS pillar-structured film could be generated through a double replica process from a rigid silicon substrate. After being modified by a monolayer of heptadecafluorodecyltrimethoxysilane (FAS), the microstructured surfaces exhibited superhydrophobicity with a water contact angle (CA) as high as 151.2 ± 1.5° and a 43° sliding angle (SA), indicating a high adhesive state.[36] Primarily, nanowires grow along the horizontal direction after placing a droplet of diluted polyvinyl-formal (PVF) solution onto this surface (Scheme 1). Following the application of unidirectional stretching force on both sides of the flexible film, the alignment of nanowires changes to random patterns and then to a totally vertical arrangement.

Figure.1a−c are representative scanning electron microscopy (SEM) images of as-prepared nanowire patterns on spindle-pillar-structured substrates with similar pillar shapes but diverse horizontal gaps. L_h and L_v are identified as the micropillar gaps in horizontal and vertical directions, respectively. L_v was fixed at 10 μm, while L_h could be changed to 10, 15, and 20 μm. When L_h and L_v were equivalent, PVF nanowires were parallel to the horizontal shrinkage direction of a droplet's three-phase contact line (TCL). As L_h increased to 15 μm, the alignment of nanowires became confused. Following the enlargement of L_h to 20 μm, no horizontal nanowires survived, while all the nanowires were oriented vertically. Figure 1d shows the nanowire formation ratio in horizontal (blue line) and vertical (orange line) directions depending on increasing L_h value. When the L_h was changed from 5 to 25 μm while L_v remained at 10 μm, horizontally formed nanowires were reduced, while vertically aligned nanowires increased dramatically.

To investigate the detailed mechanism of tunable nanowire alignment depending on unidirectionally tailored pillar gaps, the formation process of nanowires in horizontal/vertical directions should be taken into consideration. As reported in our previous study,[26] nanowires were generated from liquid bridges, which have been formed following the shrinkage of the droplet's TCL. Inside the liquid bridges, the importance of different forces relative to one another in the dynamics of narrowing and formation of nanowires is mainly dominated by two competitors. One is F_s, which represents the structural cohesive force. For a non-Newtonian fluid,[37,38] it can be expressed as

$$F_s = k\eta \frac{R_n^2}{L} \quad (1)$$

where k is the constant coefficient, η is the viscosity value of the liquid, R_n is the radius of the liquid bridge neck, and L is the gap of the micropillars (Supplemental Figure S1). F_c is capillary force, which consists of surface tension by the contact line and capillary pressure at the fluid/solid interface[39] and can be expressed as

$$F_c = F_{surface\cdot tension} + F_{Laplace\cdot press}$$

$$= 2\pi\gamma R_n + \pi\gamma R_n^2 \left(\frac{1}{R_{tp}} - \frac{1}{R_n}\right) \quad (2)$$

where R_{tp} is the meridional curvature of the meniscus surface, and γ is the surface tension of the liquid.

According to the above equations to calculate the forces inside liquid bridges, it is easy to see that the micropillar gap, L, affects only F_s, whereas it shows poor influence on F_c. Thus, F_s has been employed to calculate the force competition of liquid bridges in horizontal/vertical directions. In brief, we identify K to calculate the diverse directional F_s in order to predict the nanowire aligning direction.

$$K = \frac{(F_s)_h}{(F_s)_v} \quad (3)$$

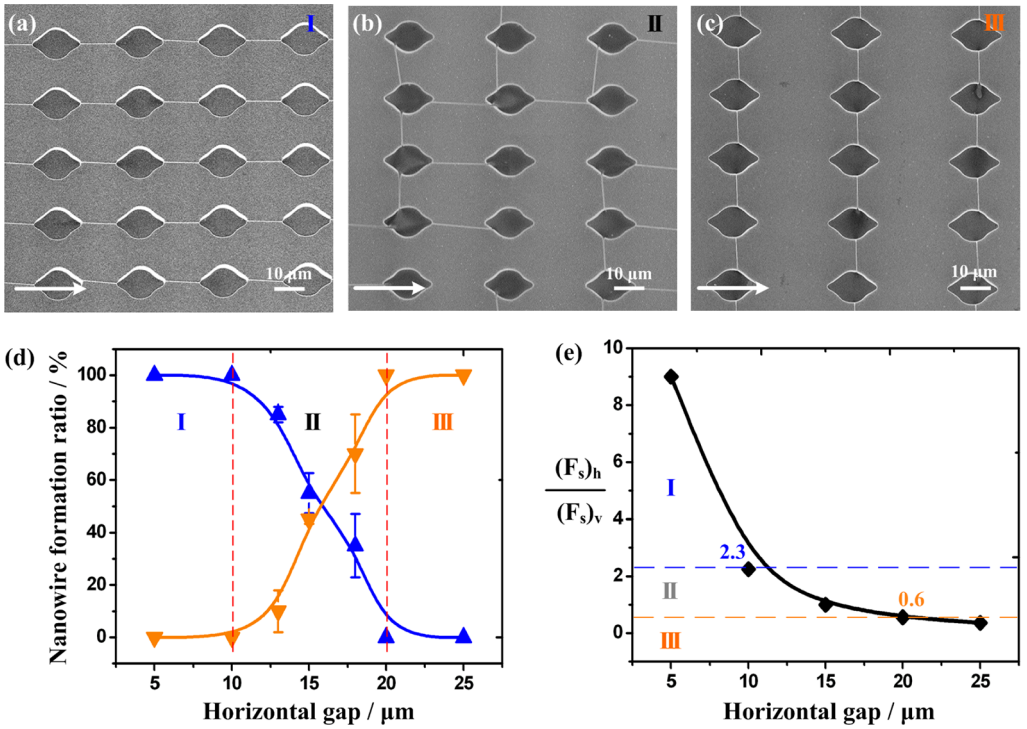

Figure 1. The competition of structural cohesive forces (F_s) inside liquid bridges generated between horizontal and vertical pillar gaps dominates the alignment of nanowires. Increasing the horizontal pillar gap (L_h) will reduce the horizontal F_s value, yielding a 90° change of nanowire orientation angle. SEM images of nanowire patterns on spindle-pillar-structured substrates with similar vertical gaps (10 μm) but L_h values of (a) 10 μm, (b) 15 μm, and (c) 20 μm. When the L_h is 10 μm, the nanowires were regularly formed in the horizontal direction. Upon increasing L_h to 15 μm, vertical nanowires appeared as well as the horizontal ones, indicating the F_s in different directions were nearly equivalent. When L_h was 20 μm, no horizontal nanowires survived, whereas all nanowires were formed in the vertical direction. (d) Dependence of nanowire formation ratio in the horizontal (blue line) and vertical (orange line) directions on L_h. Following the increase of L_h, the nanowire formation ratio in the horizontal direction was reduced, while it increased dramatically in the vertical direction. (e) The dependence of the ratio of F_s in the horizontal and vertical directions (defined as K) on L_h can be calculated, revealing the importance of F_s in predicting the nanowire alignment. When the K value is more than 2.3, nanowires might grow horizontally. If the K value is near 0.6, vertical nanowire patterns can be generated. An intermediate K value indicates random nanowire patterns.

where $(F_s)_h$ is the F_s value in the horizontal direction and $(F_s)_v$ is the F_s value in the vertical direction, which can be calculated on the basis of the L_h and L_v values (the detailed calculation can be found in Supplemental Section 2).

Figure 1e shows the relationship between K and L_h. The K value was more than 2.3 with L_h ranging from 5 to 10 μm, indicating the horizontal F_s dominated the nanowire formation and yielded aligned 1D nanostructures parallel to the TCL shrinkage direction. When the K value decreased to 0.6 by enhancing the L_v value, the nanowires grew not only in the horizontal direction but also in the vertical orientation. When the K value is less than 0.6 by increasing L_h to more than 20 μm, the vertical F_s governed this competition, resulting in aligned nanowires perpendicular to the TCL shrinkage direction. In summary, the calculated K value revealed the competition of F_s in diverse directions, providing useful information for predicting the nanowire alignment. When the K value is more than 2.3, nanowires might grow horizontally. If the K value approximates 0.6, vertical nanowire patterns can be generated. An intermediate K value indicates random nanowire patterns. Due to the additive effect of the TCL shrinkage force, the transformation point of K is 2.3 instead of 1; details can be found in Supplemental Section 2.

With an understanding of the dominating force of nanowire positioning based on calculated K values, we performed a series of smart alignments of nanowires by stretching PDMS surfaces with varying pillar arrangements. An equilateral-triangle-patterned pillar-structured surface was employed to generate tunable nanowire alignment (Figure 2a). Gaps between these three micropillars were equal (10 μm), yielding a "Y"-type nanowire pattern after TCL shrinkage of a calcein/PVF hybrid droplet (1:10, w/w). Green fluorescent nanowires (*ca.* 230 nm) were generated from each edge of the three pillars and finally converged as a joint (Figure 2b,c). In this case, the K values were equal, indicating uncontrollable nanowire patterns such as the "Y" type. Upon horizontally stretching the elastomeric substrate until the ratio of L_h/L_v is *ca.* 1.9 (Figure 2e), liquid bridges were formed only between the vertical micropillar pairs. The calculated K is *ca.* 0.62, which is close to the 0.6 transformation point, indicating vertical F_s dominates the nanowire formation.

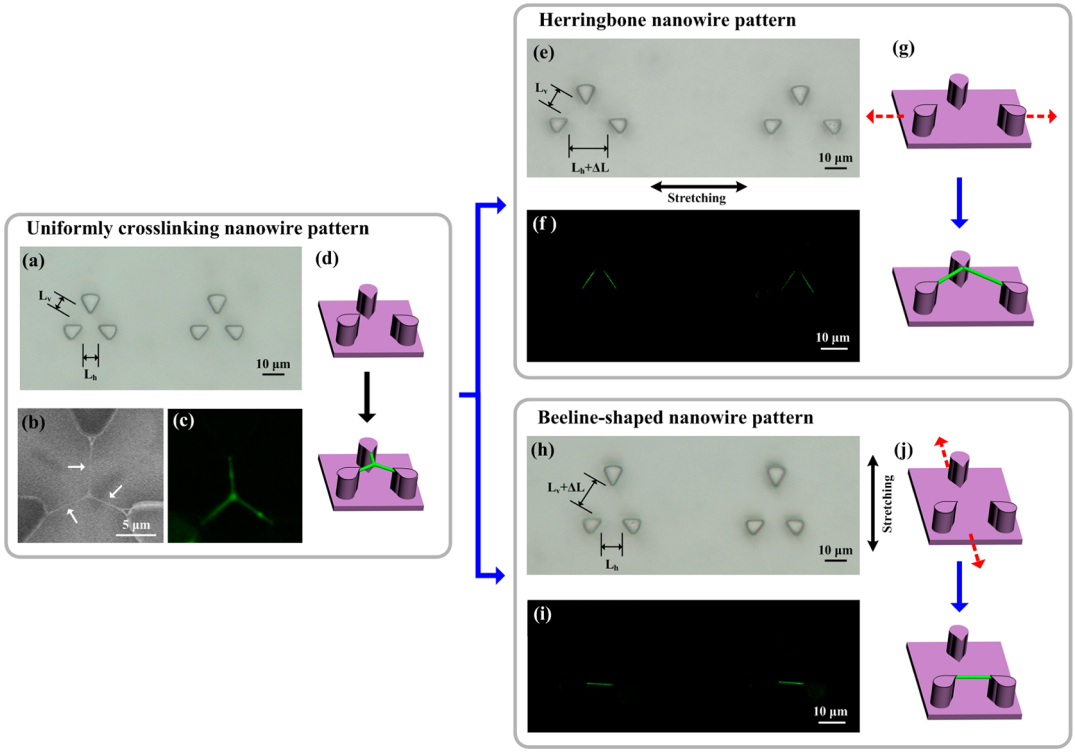

Figure 2. Tunable nanowire patterns can be generated by stretching an equilateral-triangle-patterned pillar-structured PDMS surface. Microscopically optical observation of (a) original, (e) horizontally stretched, and (h) vertically stretched equilateral-triangle-patterned micropillar arrangements. After placing a calcein/PVF hybrid droplet (1:10, w/w) onto these surfaces, diverse nanowire patterns can be formed accordingly. (b) SEM and (c) fluorescent micrograph of nanowires on (a) a surface. Owing to equal *K* values (the ratio of F_s in horizontal and vertical directions), liquid bridges were initially formed from each of the three micropillars and finally converged at a central point as a joint, yielding a "Y"-type nanowire pattern. (f and i) Fluorescent micrographs of nanowire patterns on (e) and (h), respectively. Horizontal stretching led to the *K* value decreasing to ca. 0.6; thus, herringbone-like nanowire patterns could be obtained. If the surface was stretched vertically to generate a *K* value of approximately 6.7, only one straight nanowire was generated between the horizontal micropillar pair. (d, g, and j) Corresponding schematic illustrations.

Thus, herringbone-like nanowire patterns could be obtained as shown in Figure 2f. If the surface was stretched vertically to obtain an L_h/L_v ratio of *ca.* 0.6 (Figure 2h), the *K* value was approximately 6.7, revealing that horizontal F_s governed the nanowire formation. Thus, only one straight nanowire was generated between a horizontal micropillar pair (Figure 2i). Therefore, on-demand nanowire patterns could be built by stretching a flexible PDMS surface in different directions. The tension-introduced gap changes yield a dominating F_s in different directions, which guided the nanowire alignment.

More complex nanowire alignments can be achieved by stretching a rhombus-patterned pillar-structured surface in various directions. As shown in Figure 3a, four micropillars arranged as a rhombus have equal gaps ($L_1 = L_2 = L_3 = L_4$) and relatively larger L_h and L_v. When the substrate was vertically stretched, the *K* value was calculated as nearly 2.5 (Figure 3b). As a result, only one nanowire grew between the horizontal micropillar pair (Figure 3c). One straightly aligned nanowire bridged the two micropillar tips in order to get a maximum F_s to compete with the destructive F_c. Figure 3d is an optical microscopic observation of a diagonally stretched substrate. Four micropillars were separated into two pairs with a *K* value of *ca.* 5.1 (note that the *K* value of L_1 to L_v or L_h was even higher in this case). Therefore, nanowires could be generated only between the two pairs of micropillars. Figure 3e shows as-prepared nanowires are parallel to each other, bridging diagonal micropillar pairs. Other nanowire patterns could also be formed by asymmetrically stretching the substrate. As shown in Figure 3f, upon stretching the substrate along both side arrows labeled on the image, the *K* ratio of L_1 to L_3, L_v, or others was lower than 0.4, yielding nanowires growing in a herringbone shape (Figure 3g). In the case of asymmetrically stretching the substrate in a diagonal direction (Figure 3h), the L_1 value became smaller than the other five gaps (the *K* value was lower than 0.3, revealing that only one nanowire might grow on the top left of the micropillar pattern (Figure 3i)). In summary, complex nanowire alignments can be achieved by selectively stretching the flexible PDMS surface, exhibiting the generality and efficiency of this technique.

Besides single stretching, double-stretching processes in different directions can also be performed, yielding a square nanowire loop with alternative green and orange fluorescence by placing liquid droplets with different compositions. A square-pillar-structured

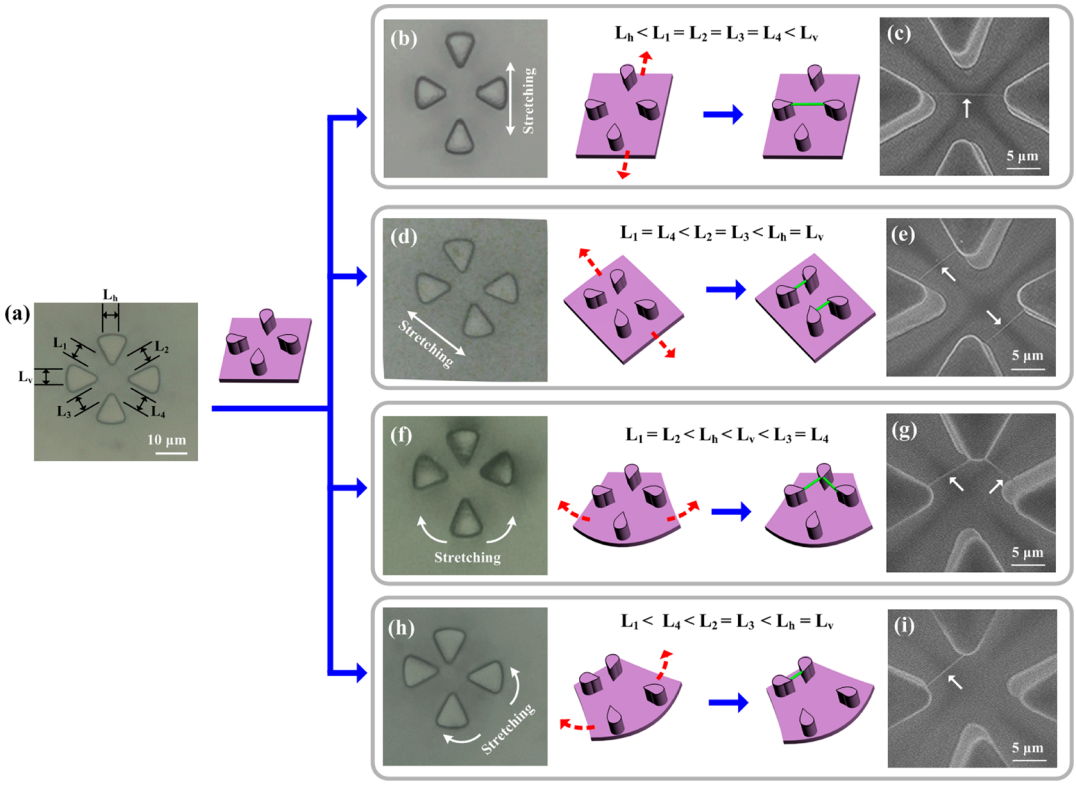

Figure 3. Through diverse strategies to stretch the substrate, complex nanowire patterns can be generated upon the same rhombus-patterned pillar-structured PDMS surface. Microscopic optical observation of (a) original, (b) vertically stretched, (d) diagonally stretched, (f) asymmetrically stretched, and (h) one side stretched rhombus-patterned micropillar arrangements. The white arrows show the stretching directions. After placing a calcein/PVF hybrid droplet (1:10, w/w) onto these surfaces, diverse nanowire patterns can be formed accordingly. (c, e, g, i) Corresponding nanowire patterns on (b), (d), (f), and (h) surfaces, respectively. Owing to tension-induced *K* value changes, the dominating structural cohesive force (F_s) will be different under different stretching models. Thus, (c) one nanowire bridging the horizontal micropillar pair, (e) parallel nanowires between the two pairs of diagonal micropillars, (g) herringbone-shaped nanowires, and (i) only one nanowire grown on the top left of the micropillar pattern can be generated on the same pillar-structured PDMS surface.

PDMS surface was employed in this patterning process (Figure 4a). Primarily, horizontally aligned nanowires could be generated through stretching the surface vertically. The calcein-doped PVF droplet might endow the nanowires (*ca.* 227 nm) with green fluorescence. Owing to the high *K* value (more than 5.1), two green nanowires were aligned horizontally, parallel to each other. Then, the nanowire-loading surface was stretched horizontally until the *K* value was lower than 0.4. The polymeric 1D nanostructures were so flexible that they survived during this process. A droplet of rhodamine B-doped PVF solution (rhodamine B/PVF = 1:10, w/w) was placed onto the shape-shifted surface. Two vertical nanowires with orange fluorescence were thus generated, whereas the horizontal green ones remained. To avoid the spreading of rhodamine B-doped PVF solution onto the calcein/PVF nanowires, a secondary modification of FAS on the calcein/PVF 1D nanostructures has to be performed. Owing to the low surface free energy of the modified calcein/PVF nanowires, the secondary polymeric solution shrinks and forms parallel nanowires only in the vertical direction. Therefore, by utilizing double-stretching behaviors in diverse directions, nanowires consisting of various compositions might selectively grow in designed positions (Figure 4b).

Since the calcein can be quenched by ferric compounds while rhodamine B loses its fluorescence when contacting iodine, such loop-structured alternative nanowires might serve as an encoded sensor based on selective quenching reactions. Three kinds of ethanol solutions, containing ferric nitrate (0.01 wt %) or iodine (0.01 wt %) and their mixture at equal weight, have been prepared, respectively. Then, each solution was carried by a beam of nitrogen and blown toward alternative loop-structured nanowires. Tiny ethanol drops, containing ferric nitrate or iodine, condense on the nanowires and undergo a quenching reaction with proper fluorescent molecules. Figure 4c shows the result of alternative loop-structured nanowires contacting an ethanol fog containing ferric nitrate. Since the ferric compounds reacted only with calcein molecules, green fluorescent nanowires become dark, while orange ones (rhodamine B) survive, indicating a selective quenching reaction occurring on the nanowire patterns. Once exposed to the ethanol fog containing iodine, such alternative loop-structured nanowires show only horizontal green fluorescence (Figure 4d). When exposed to

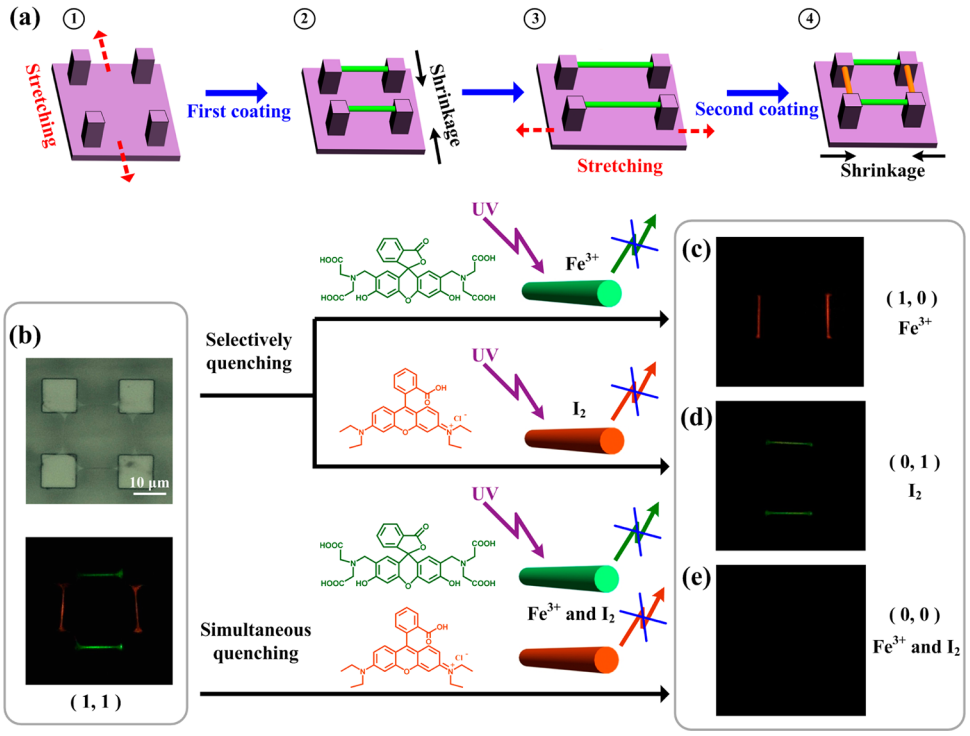

Figure 4. A square nanowire loop consisting of alternative calcein/rhodamine B can be generated through double-stretching processes and might serve as an encoded sensor based on selective quenching reactions. (a) Schematic illustration of the fabrication process. Upon stretching the substrate vertically and drawing with a calcein-doped droplet, two green nanowires were aligned horizontally owing to the high *K* value (more than 5.1). Then, the nanowire-loaded surface was stretched horizontally until the *K* value was less than 0.4. Two vertical nanowires with orange fluorescence were then generated by placing a droplet of rhodamine B-doped PVF solution (rhodamine B/PVF = 1:10, w/w) onto the shape-shifted surface. (b) Optical and fluorescent micrographs of a closed nanowire loop with alternative compositions through double-stretching processes. To avoid the spreading of rhodamine B-doped PVF solution onto the calcein/PVF nanowires, a secondary modification of FAS on the calcein/PVF 1D nanostructures has to be performed. Following the condensation of ferric or iodine compounds, a selective detecting process can be performed. Through introduction of different target compounds, fluorescent nanowires could be selectively or totally quenched. (c) By employing an ethanol fog containing ferric nitrate, calcein nanowires were quenched, whereas rhodamine B ones survived. (d) When exposed to a mixed iodine fog, orange rhodamine B nanowires were quenched, leaving only green fluorescence. (e) When exposed to an ethanol fog carrying a ferric compound and iodine, both green and red fluorescence became dark.

an ethanol fog containing ferric nitrate and iodine mixture, all the nanowires quenched to dark. Therefore, alternative nanowire loops generated by this stretching strategy showed a selective detection of diverse target compounds and could serve as an organically encoded sensor.

Such alternative nanowire patterns could also be transferred from pillar-structured surfaces to flat films. Figure 5a shows the transfer process of a nanowire matrix. Through a double-stretching process, an alternative nanowire matrix has been generated consisting of horizontal green nanowires (calcein) and vertical orange ones (rhodamine B). Then, after pressing a hot and flat PDMS film onto the nanowire matrix and keeping contact for 2 min, such alternative nanowire patterns could be transferred by peeling the film carefully. Figure 5b,c are optical and fluorescent observations of a transferred alternative nanowire matrix on a flat PDMS film. Since nanowires generated through our approach were well-organized and easily transferred, this stretching strategy will put forward a practical application for 1D nanostructures integrated into

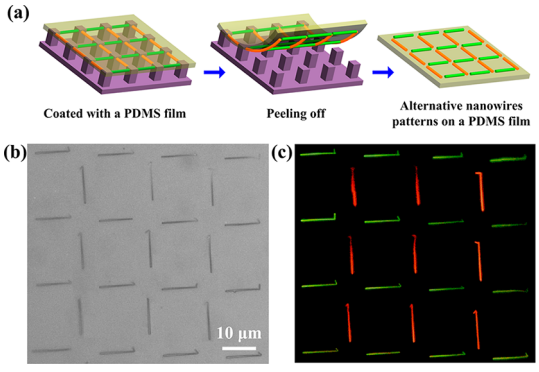

Figure 5. Alternative nanowire patterns could be transferred from pillar-structured surfaces to flat films. (a) Schematic illustration of the transfer process. Through a double-stretching process, an alternative nanowire matrix has been generated consisting of horizontal green nanowires (calcein) and vertical orange ones (rhodamine B). Then, after pressing a hot and flat PDMS film onto the nanowire matrix and keeping contact for 2 min, such alternative nanowire patterns could be transferred by peeling the film carefully. (b) Optical and (c) fluorescent images of an alternative nanowire matrix transferred onto a flat PDMS film. The calcein nanowires were oriented in the horizontal direction, whereas the rhodamine B ones were aligned vertically.

microcircuits, sensitive sensors, and other organic functional nanodevices.

CONCLUSION

In conclusion, a simple yet efficient approach for smart alignment of nanowires has been developed by stretching a PDMS pillar-structured surface in diverse directions. External tension behavior introduced a change in the micropillar gaps on the PDMS film; thus, the structural cohesive forces inside the liquid bridges in different directions were changed accordingly. Dominating structural cohesive forces will favor the nanowire aligning in its direction, yielding on-demand nanowire alignments. Remarkably, a square nanowire loop with alternative compositions can be generated through double-stretching processes. Such nanowire patterns can also be achieved *via* reported methods such as electric/magnetic-field-assisted electrospinning;[12,13] however, high-cost equipment or complex procedures are required. Our strategy provides a facile, low-cost, yet efficient route to overcome the above limitations. Importantly, this nanowire loop might serve as an encoded sensor based on selective quenching effects. Furthermore, such alternative nanowire patterns can be transferred from pillar-structured surfaces to flat films. Thus, we anticipate this stretching technique will lead to hierarchical assembly of organic 1D nanostructures with different compositions and integration into functional device applications.

EXPERIMENTAL SECTION

Smart Alignment of Nanowires by Stretching a PDMS Surface. Flexible PDMS pillar-structured surfaces can be obtained through a hot embossing technique. The modification of superhydrophobic PDMS surfaces can be found in our previous studies.[26] The stretching of the PDMS surfaces was performed by a man-made pulling apparatus (see Supplemental Figure S3). Notably, the pillar-structured PDMS substrates were primarily stretched at a certain degree and then fixed statically. Droplets of PVF solution (10^{-3}, w/w) or calcein/rhodamine B-doped PVF solution (calcein or rhodamine B/PVF = 1:10, w/w) were carefully placed onto the stretched substrates, yielding on-demand nanowire alignments. Nanowires were inclined to a position between the closer micropillars. In the double-stretching processes, to avoid the spreading of rhodamine B-doped PVF solution onto the calcein/PVF nanowires, a secondary modification of FAS on the calcein/PVF 1D nanostructures has been performed. Owing to the low surface free energy of the modified calcein/PVF nanowires, the secondary polymeric solution shrinks and forms parallel nanowires only in the vertical direction. Thus, a square nanowire loop with alternative compositions could be generated.

Instruments and Characterization. The structures of suspended nanowire patterns were investigated by scanning electron microscopy (JEOL, JSM-6700F, Japan) at an accelerating voltage of 3.0 kV. Static contact angles were measured on a Dataphysics OCA20 contact-angle system at ambient temperature. The average CA was obtained by measuring more than five different positions of the same sample. The optical and fluorescent micrographs of aligned calcein nanowire patterns were investigated through an optical microscope (Vision Engineering Co., UK), which was coupled to a CCD camera and connected to a desktop computer.

Conflict of Interest: The authors declare no competing financial interest.

Acknowledgment. The authors thank the National Research Fund for Fundamental Key Projects (2009CB930404, 2010CB934700, 2011CB935700, 2012CB933200), the National Natural Science Foundation (21201169, 20974113, 21071148, 20920102036, 21121001, 91127025, 51173099), and the Key Research Program of the Chinese Academy of Sciences (KJZD-EW-M01) for financial support.

Supporting Information Available: The formation process of aligned nanowires, calculated details of F_s inside liquid bridges in horizontal/vertical directions, and the setup of a man-made stretching apparatus. This material is available free of charge *via* the Internet at http://pubs.acs.org.

REFERENCES AND NOTES

1. Tang, Z. Y.; Kotov, N. A.; Giersig, M. Spontaneous Organization of Single CdTe Nanoparticles into Luminescent Nanowires. *Science* **2002**, *297*, 237–240.
2. Takahashi, T.; Nichols, P.; Takei, K.; Ford, A. C.; Jamshidi, A.; Wu, M. C.; Ning, C. Z.; Javey., A. Contact Printing of Compositionally Graded CdS_xSe_{1-x} Nanowire Parallel Arrays for Tunable Photodetectors. *Nanotechnology* **2012**, *23*, 045201.
3. Heath, J. R.; Kuekes, P. J.; Snider, G. S.; Williams, R. S. A Defect-Tolerant Computer Architecture: Opportunities for Nanotechnology. *Science* **1998**, *280*, 1716–1721.
4. Hu, J. T.; Odom, T. W.; Lieber, C. M. Chemistry and Physics in One Dimension: Synthesis and Properties of Nanowires and Nanotubes. *Acc. Chem. Res.* **1999**, *32*, 435–445.
5. Lu, W.; Lieber, C. M. Nanoelectronics from the Bottom Up. *Nat. Mater.* **2007**, *6*, 841–850.
6. Liu, J. W; Liang, H. W; Yu, S. H. Macroscopic-Scale Assembled Nanowire Thin Films and Their Functionalities. *Chem. Rev.* **2012**, *112*, 4770–4799.
7. Shi, Y. H; Hu, B; Yu, X. C; Zhao, R. L; Ren, X. F; Liu, S. L; Liu, J. W; Feng, M; Xu, A. W; Yu, S. H. Ordering of Disordered Nanowires: Spontaneous Formation of Highly Aligned, Ultralong Ag Nanowire Films at Oil−Water−Air Interface. *Adv. Funct. Mater.* **2010**, *20*, 958–964.
8. Liu, J. W; Zhu., J, H; Zhang, C. L; Liang, H. W; Yu, S. H. Mesostructured Assemblies of Ultrathin Superlong Tellurium Nanowires and Their Photoconductivity. *J. Am. Chem. Soc.* **2010**, *132*, 8945–8952.
9. Liu, J. W; Xu., J.; Liang, H. W.; Wang, K.; Yu, S. H. Macroscale Ordered Ultrathin Telluride Nanowire Films; and Tellurium/Telluride Hetero-Nanowire Films. *Angew. Chem., Int. Ed.* **2012**, *51*, 7420–7425.
10. Huang, Y.; Duan, X. F.; Wei, Q. Q.; Lieber, C. M. Directed Assembly of One-Dimensional Nanostructures into Functional Networks. *Science* **2001**, *291*, 630–633.
11. Dvir, T.; Timko, B. P.; Kohane, D. S.; Langer, R. Nanotechnological Strategies for Engineering Complex Tissues. *Nat. Nanotechnol.* **2011**, *6*, 13–22.
12. Li, D.; Wang, Y. L.; Xia, Y. N. Electrospinning Nanofibers as Uniaxially Aligned Arrays and Layer-by-Layer Stacked Films. *Adv. Mater.* **2004**, *16*, 361–366.
13. Yang, D. Y.; Lu, B.; Zhao, Y.; Jiang, X. Y. Fabrication of Aligned Fibirous Arrays by Magnetic Electrospinning. *Adv. Mater.* **2007**, *19*, 3702–3706.
14. Lin, Z. Q.; Granick, S. Patterns Formed by Droplet Evaporation from a Restricted Geometry. *J. Am. Chem. Soc.* **2005**, *127*, 2816–2817.
15. Pisula, W.; Menon, A.; Stepputat, M.; Lieberwirth, I.; Kolb, U.; Tracz, A.; Sirringhaus, H.; Pakula, T.; Müllen, K. A Zone-Casting Technique for Device Fabrication of Field-Effect Transistors Based on Discotic Hexa-Peri-Hexabenzocoronene. *Adv. Mater.* **2005**, *17*, 684–689.
16. Hameren, R. V; Schön, P.; Buul, A. M.; Hoogboom, J.; Lazarenko, S. V.; Gerritsen, J. W.; Engelkamp, H.; Christianen, C. M.; Heus, H. A.; Maan, J. C.; *et al.* Macroscopic Hierarchical

Surface Patterning of Porphyrin Trimers *via* Self-Assembly and Dewetting. *Science* **2006**, *314*, 1433–1436.
17. Chou, S. Y.; Krauss, P. R.; Renstrom, P. J. Imprint Lithography with 25-Nanometer Resolution. *Science* **1996**, *272*, 85–87.
18. Hu, Z. J.; Muls, B.; Gence, L.; Serban, D. A.; Hofkens, J.; Melinte, S.; Nysten, B.; Demoustier-Champagne, S.; Jonas, A. M. High-Throughput Fabrication of Organic Nanowire Devices with Preferential Internal Alignment and Improved Performance. *Nano. Lett* **2007**, *7*, 3639–3644.
19. Hung, A. M.; Stupp, S. I. Simultaneous Self-Assembly, Orientation, and Patterning of Peptide-Amphiphile Nanofibers by Soft Lithography. *Nano. Lett* **2007**, *7*, 1165–1171.
20. Tao, A.; Kim, F.; Hess, C.; Goldberger, J.; He, R. R.; Sun, Y. G.; Xia, Y. N.; Yang, P. D. Langmuir-Blodgett Silver Nanowire Monolayers for Molecular Sensing Using Surface-Enhanced Raman Spectroscopy. *Nano. Lett.* **2003**, *3*, 1229–1233.
21. Jin, S.; Whang, D. M.; McAlpine, M. C.; Friedman, R. S.; Wu, Y.; Lieber, C. M. Scalable Interconnection and Integration of Nanowire Devices without Registration. *Nano Lett.* **2004**, *4*, 915–919.
22. Li, X. L.; Zhang, L.; Wang, X. R.; Shimoyama, I.; Sun, X. M.; Seo, W. S.; Dai, H. J. Langmuir-Blodgett Assembly of Densely Aligned Single-Walled Carbon Nanotubes from Bulk Materials. *J. Am. Chem. Soc.* **2007**, *129*, 4890–4891.
23. Duan, X. F.; Niu, C. M.; Sahi, V.; Chen, J.; Parce, J. W.; Empedocles, S.; Goldman, J. L. High-Performance Thin-Film Transistors Using Semiconductor Nanowires and Nanoribbons. *Nature* **2003**, *425*, 274–278.
24. Yan, C. Y.; Zhang, T.; Lee, P. S. Flow Assisted Synthesis of Highly Ordered Silica Nanowire Arrays. *Appl. Phys. A: Mater. Sci. Process.* **2009**, *94*, 763–766.
25. Yu, G.; Cao, A.; Lieber, C. M.; Yu, G.; Cao, A.; Lieber, C. M. Large-Area Blown Bubble Films of Aligned Nanowires and Carbon Nanotubes. *Nat. Nanotechnol.* **2007**, *2*, 372–377.
26. Su, B.; Wang, S. T.; Ma, J.; Wu, Y. C.; Chen, X.; Song, Y. L.; Jiang, L. Elaborate Positioning of Nanowire Arrays Contributed by Highly Adhesive Superhydrophobic Pillar-Structured Substrates. *Adv. Mater.* **2012**, *24*, 559–564.
27. Su, B.; Wang, S. T.; Wu, Y. C.; Chen, X.; Song, Y. L.; Jiang, L. Small Molecular Nanowire Arrays Assisted by Superhydrophobic Pillar-Structured Surfaces with High Adhesion. *Adv. Mater.* **2012**, *24*, 2780–2785.
28. Yan, X.; Yao, J. M.; Lu, G.; Li, X.; Zhang, J. H.; Han, K.; Yang, B. Fabrication of Non-Close-Packed Arrays of Colloidal Spheres by Soft Lithography. *J. Am. Chem. Soc.* **2005**, *127*, 7688–7689.
29. Wang, C. Y.; Zheng, W.; Yue, Z. L.; Too, C. O.; Wallace, G. G. Buckled Stretchable Polypyrrole Electrodes for Battery Applications. *Adv. Mater.* **2011**, *23*, 3580–3584.
30. Yu, C. J.; Masarapu, C.; Rong, J. P.; Wei, B. Q.; Jiang, H. Q. Stretchable Supercapacitors Based on Buckled Single-Walled Carbon-Nanotube Macrofilms. *Adv. Mater.* **2009**, *21*, 4793–4797.
31. Qi, Y.; Kim, J.; Nguyen, T. D.; Lisko, B.; Purohit, P. K.; McAlpine, M. C. Enhanced Piezoelectricity and Stretchability in Energy Harvesting Devices Fabricated from Buckled PZT Ribbons. *Nano. Lett.* **2011**, *11*, 1331–1336.
32. Kumar, G.; Tang, H. X.; Schroers, J. Nanomoulding with Amorphous Metals. *Nature* **2009**, *457*, 868–872.
33. Hu, J. T.; Ouyang, M.; Yang, P. D.; Lieber, C. M. Controlled Growth and Electrical Properties of Heterojunctions of Carbon Nanotubes and Silicon Nanowires. *Nature* **1999**, *399*, 48–51.
34. Nagashima, K.; Yanagida, T.; Tanaka, H.; Seki, S.; Saeki, A.; Tagawa, S.; Kawai, T. Effect of the Heterointerface on Transport Properties of *in Situ* Formed MgO/Titanate Heterostructured Nanowires. *J. Am. Chem. Soc.* **2008**, *130*, 5378–5382.
35. Penn, S. G.; He, L.; Natan, M. J. Nanoparticles for Bioanalysis. *Curr. Opin. Chem. Biol.* **2003**, *7*, 609–615.
36. Su, B.; Wang, S. T.; Ma, J.; Song, Y.; Jiang, L. "Clinging-Microdroplet" Patterning upon High-Adhesion, Pillar-Structured Silicon Substrates. *Adv. Funct. Mater.* **2011**, *21*, 3297–3307.
37. Miranda, J. A. Shear-Induced Effects in Confined Non-Newtonian Fluids under Tension. *Phys. Rev. E* **2004**, *69*, 016311.
38. Verbeeten, W. M. H. Non-Linear Viscoelastic Models for Semi-Flexible Polysaccharide Solution Rheology over a Broad Range of Concentrations. *J. Rheol.* **2010**, *54*, 447–470.
39. Bhat, P. P.; Appathurai, S.; Harris, M. T.; Pasquali, M.; McKinley, G. H.; Basaran, O. A. Formation of Beads-On-A-String Structures During Break-Up of Viscoelastic Filaments. *Nat. Phys.* **2010**, *6*, 625–631.